J. Biomechanics, 1976, Vol. 9, pp. 377–386. Pergamon Press. Printed in Great Britain

NONLINEAR BEHAVIOR OF THE HUMAN INTERVERTEBRAL DISC UNDER AXIAL LOAD*

R. F. KULAK, T. B. BELYTSCHKO and A. B. SCHULTZ

Department of Materials Engineering, University of Illinois at Chicago Circle, Chicago, IL 60680, U.S.A.

and

J. O. GALANTE

Department of Orthopaedic Surgery, Rush-Presbyterian-St. Luke's Hospital, Chicago, IL 60612, U.S.A.

Abstract—The nonlinear, rate-independent behavior of human intervertebral discs is studied with a finite element model which incorporates a nonlinear elastic constitutive relation for the annulus fibrosis. The elastic coefficients and a nonlinear constitutive parameter for the annulus fibrosis were obtained by matching experimental results for the disc's load–deflection behavior. The axisymmetric finite element model includes the annulus, end plates, portions of the vertebral bodies and an incompressible nucleus pulposus. Results for annulus bulging, internal pressures, and response variations due to level-to-level changes in geometry are in agreement with available experimental data. It is shown that there are marked differences in the compressive behavior of lumbar and thoracic discs. In addition, two types of degeneration, one characterized by annular tears, the other by a desiccated nucleus, are studied.

INTRODUCTION

The human intervertebral disc is an essential element in sustaining weight and in permitting mobility of the spine. In normal activities, it is subjected to considerable mechanical stresses, which may be an important factor in disc degeneration and other acute and chronic spinal injuries. Yet our understanding of the mechanical behavior of the disc is at best fragmentary. Kraus *et al.* (1972), presented some interesting results on comparisons of analytically predicted zones of high shear stresses in torsion and the location of annular tears. Belytschko *et al.* (1974) employed a finite element model for the study of stress distributions and deformation behavior of axially loaded discs, both normal and with specific types of degeneration. It was found in the latter study that the material anisotropy in discs is so pronounced that in the study of axial compression, its omission leads to errors of 50% in important characteristics such as nuclear pressure. It was also found that a linear analysis will not adequately explain differences between thoracic and lumbar disc behavior or the differences between tensile and compressive response.

In this study, a nonlinear time-independent constitutive relationship is developed for the annulus fibrosis so that these discrepancies between the model and experimental results can be resolved. The form of the stress–strain law for the annulus fibrosis of the disc was obtained by considering the substructure of the annulus and the reported behavior of collagen fibers. Values of the required material constants were then found by matching experimental load–deflection curves. The resulting model reproduces other experimental results, such as nuclear pressure, level-to-level variations, and bulge values quite well. Results are presented for stress distributions and response differences under tension and compression. In addition, the model is used to simulate two types of disc degeneration: one characterized by annular tears, the other by a desiccated nucleus.

* *Received* 20 *October* 1975.

RELATED LITERATURE

Gross disc behavior

Axial force–deflection properties of intervertebral discs have been reported by several investigators. For instance, Virgin (1951) tested single discs attached to thin slices of their inferior and superior vertebrae in compression. He presented load–deflection curves which exhibited various degrees of nonlinear behavior and reported that the intervertebral disc behaves visco-elastically.

Brown *et al.* (1957) conducted axial compression tests on fresh vertebra–disc–vertebra segments of the lumbosacral spine with the posterior elements removed. Rolander (1966) performed a series of mechanical tests on lumbar discs and by macroscopic examination classified the excised discs according to degree of degeneration. The reported compression curves for normal and degenerate discs show that, for equal load levels, the degenerate discs deflect much more than the normal discs.

Markolf (1972) conducted axial compression and tension tests, among other tests, on thoracolumbar discs. His results indicate that there are significant differences in behavior between lumbar and thoracic discs. In addition, each disc shows differences in response between tensile and compressive loading. Markolf also reported that intervertebral discs behave visco-elastically.

Constitutive relations for biological materials

Galante (1967) experimentally established that the annulus fibrosis is inhomogeneous and anisotropic and that it exhibits hardening stress–strain characteristics.

A number of rheological studies have been concerned with constitutive representations of the complex macroscopic mechanical properties of soft biological tissue such as that found in the annulus fibrosis. Mitton (1945) found that a power term relation between load and extension fit his experimental data from commercially tanned leather fibers. Subsequently, Morgan (1960), Elden (1968) and Blatz (1969) used power term stress–strain relations to fit their experimental data from leather collagen fibers, rat tail tendons, and human papillary muscle, respectively.

Fung (1968) suggested that the stress in some biological materials can be separated into an elastic part and a history-dependent part. He proposed an exponential form to represent the elastic stress–strain behavior of rabbit mesentery. For the history-dependent part he suggested a hereditary integral explicity dependent upon the elastic stress.

A major constituent of the annulus fibrosis is the collagen fiber bundle. Haut and Little (1972) tested the tendons of rat tails, which are a source of almost pure collagen fiber bundles, to determine the stress–strain response of collagen. To describe the stress–strain history relations, they used the quasi-linear viscoelasticity relation proposed by Fung. The elastic component of stress was found to be proportional to the square of the strain.

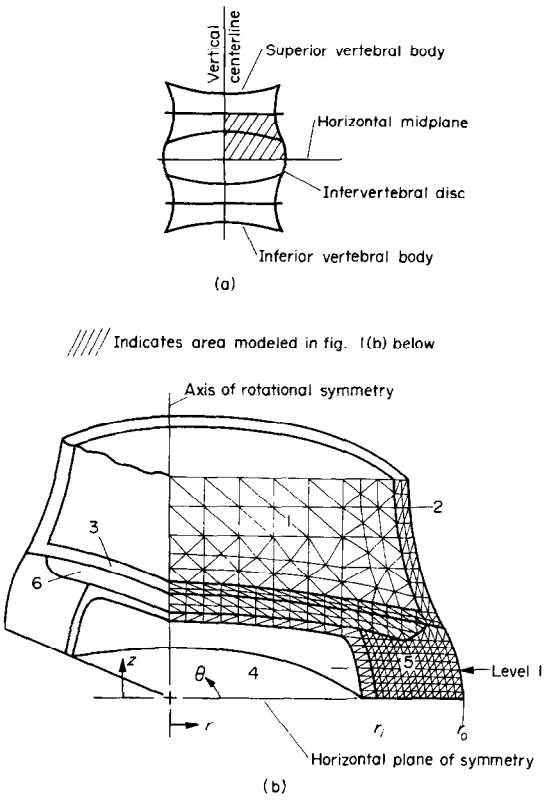

Fig. 1. (a). Vertebra–disc–vertebra unit. (b) Finite element model for unit. Due to symmetries, only the cross hatched area of (a) was modeled. The six regions represent the following components: (1) the vertebral body core of trabecular bone, (2) the vertebra's thin outer shell of cortical bone, (3) the bony end plate, (4) the nucleus pulposus, (5) the annulus fibrosus, and (6) the cartilagenous end plate.

MATERIALS AND METHODS

Nonlinear elastic constitutive relation

In this investigation we are concerned with the time independent, elastic part of the stress–strain law. Although it is recognized that viscoelasticity and creep play a significant role in the response of discs, it can be seen from the experimental results in Fig. 2 that the time independent behavior is reproducible and indicative of behavior with moderate rates of loading, such as encountered in lifting. The nonlinearity of the axial load–deflection curves of intervertebral discs is assumed to be caused primarily by the nonlinear elastic behavior of the annulus fibrosis. This assumption is made because: (1) the nucleus behaves as an incompressible, hydrostatic material; (2) the end plates are composed of cortical bone which exhibits almost linear behavior for the loads considered here; and (3) for axial loads of magnitudes found *in vivo*, vertical deflections are small enough so that nonlinear geometric effects are negligible.

When discs are compressed, the annulus fibrosis is subjected to complex states of stress because of its interaction with the incompressible nucleus. A realistic study of the behavior of the disc thus requires the employment of a three-dimensional stress–strain relation.

In developing three-dimensional stress–strain relations, forms which are inconsistent from an energy viewpoint should be avoided. Therefore, a stress–strain relation derivable from a positive definite strain energy density function is used in the present studies to represent the three-dimensional, nonlinear elastic behavior of the annulus fibrosis. It may also be applicable to other biological materials.

Let the strain energy density function, U, be given by the general form

$$U = K^{\lambda}(\epsilon_i), \tag{1}$$

where K is a scalar-valued function of the strains ϵ_i, and λ is a nonnegative constant. Specifically let $K(\epsilon_i)$ be given in reduced index notation (repeated subscripts denote summation) by

$$K = C_{ij}\epsilon_i\epsilon_j, \tag{2}$$

where C_{ij} is a set of elastic coefficients and ϵ_i are the components of the strain tensor. For a rotationally symmetric problem in cylindrical coordinates,

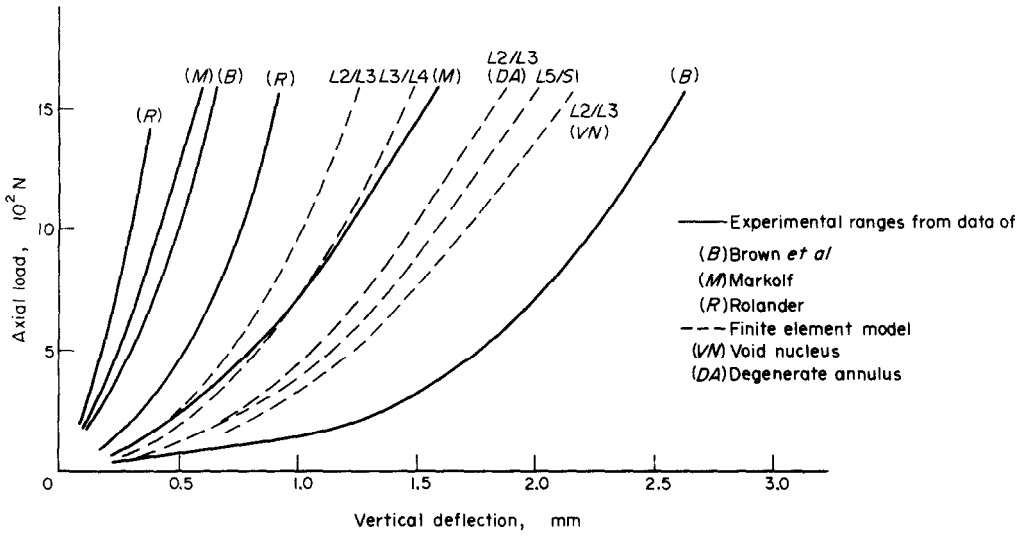

Fig. 2. Comparison between model-predicted and reported experimental load–deflection curves for normal and degenerate lumbar discs. Brown *et al.* range is for discs from *L2/L3* to *L4/L5*; Markolf's range is for discs *L1/L2* and *L2/L3*; Rolander's range is from *L2/L3* to *L5/S1*. Finite element results are for discs *L2/L3*, *L3/L4*, and *L5/S1*.

the stresses and strains are given by

$$\sigma_i = \begin{Bmatrix} \sigma_r \\ \sigma_\theta \\ \sigma_z \\ \sigma_{rz} \end{Bmatrix}, \qquad \epsilon_i = \begin{Bmatrix} \epsilon_r \\ \epsilon_\theta \\ \epsilon_z \\ 2\epsilon_{rz} \end{Bmatrix}. \tag{3}$$

The stresses are determined from the relation (see, e.g. Fung, 1965).

$$\sigma_k = \frac{\partial U}{\partial \epsilon_k} \tag{4}$$

which when applied to equation (1) gives

$$\sigma_k = \lambda K(\epsilon_i)^{\lambda-1} \frac{\partial K(\epsilon_i)}{\partial \epsilon_k}. \tag{5}$$

Using the form for K proposed in equation (2) and assuming C_{ij} is symmetric, the following stress–strain relationship is obtained

$$\sigma_k = 2\lambda K^{\lambda-1} C_{kl}\epsilon_l. \tag{6}$$

The scalar coefficient, $2\lambda K^{\lambda-1}$, depends upon the state of strain and can serve to model hardening behavior. Equation (6) yields a set of strain dependent coefficients C^*_{kl} given by

$$C^*_{kl} = 2\lambda K^{\lambda-1} C_{kl}. \tag{7}$$

The parameter λ determines the degree of nonlinearity for the elastic coefficients C^*_{kl}. If $K < 1$, whenever λ lies in the range, $0 < \lambda < 1$, it has the effect of producing a softening stress–strain curve, while for $\lambda > 1$, the stress–strain curve hardens. For the special case $\lambda = 1$, the nonlinear elastic coefficients reduce to the linear elastic coefficients.

For purposes of checking the validity of proposed stress–strain laws, note that the form chosen for $K(\epsilon_i)$, equation (2), is quadratic. A necessary and sufficient condition for a quadratic form to be positive definite is that the principal minors, which consist of the determinants of the $n \times n$ matrices in the top left-hand corner of C_{ij} ($n = 1$ to N), are all positive (see, e.g. Noble, 1969). The annulus fibrosis will here be considered orthotropic. Since the nonlinear coefficients C^*_{kl} differ from the linear coefficients C_{kl} by a scalar multiplier, both matrices are of the form given by Jayne and Suddarth (1966) for linear orthotropic materials

$$C_{ij} = \begin{bmatrix} C_{rr} & C_{r\theta} & C_{rz} & 0 \\ & C_{\theta\theta} & C_{\theta z} & 0 \\ & & C_{zz} & 0 \\ \text{symmetric} & & & C_{rz} \end{bmatrix}. \tag{8}$$

The necessary and sufficient conditions for positive definiteness lead to the following restrictions on the elastic coefficients, C_{ij}:

$$\left.\begin{gathered} C_{rr} > 0 \\ C_{rr}C_{\theta\theta} - C_{r\theta} > 0 \\ C_{rr}(C_{\theta\theta}C_{zz} - C_{\theta z}) + C_{r\theta}(C_{\theta z}C_{rz} - C_{r\theta}C_{zz}) \\ + C_{rz}(C_{\theta z}C_{r\theta} - C_{\theta\theta}C_{rz}) > 0 \\ C_{rz} > 0 \end{gathered}\right\}. \tag{9}$$

These conditions were satisfied by the material constants proposed here.

The differential form of equation (5), which is used for the incremental loading computations performed in this study, is

$$d\sigma_k = C^t_{kr}\, d\epsilon_r, \tag{10}$$

where

$$C^t_{kj} = 2\lambda\left[(\lambda - 1)K^{\lambda-2}\frac{\partial K}{\partial \epsilon_j}C_{kl}\epsilon_l + K^{\lambda-1}C_{kj}\right]. \tag{11}$$

The substructure of the annulus fibrosis must be considered in a stress–strain relationship. The annulus fibrosis is formed by a series of concentric encircling lamellae (Fick, 1904–1911; Beadle, 1931), each of which consists of collagenous fibers embedded in an amorphous ground substance. The fibers provide directional tensile strength while the ground substance serves to bond the fibers. In each lamella, the fibers run in a single direction and in alternate lamellae they are aligned at approx. $\pm 30°$ from the circumferential direction, according to Horton (1958). The mechanical response of this fiber-reinforced composite will differ depending on whether the strain in the fiber direction is tensile or compressive. In tension, the fibers provide considerable stiffness, whereas their stiffness in compression is small, and to accurately model the disc, these differences must be taken into account. A detailed description of the treatment of orthotropy and tension–compression differences is given in Appendix A.

Finite element model

A finite element model identical to that described by Belytschko *et al.* (1974) was used in this study, but with a different computational technique. This technique is described in Appendix B. The anterior components of a disc unit (the intervertebral disc and adjacent vertebral bodies) were idealized as a three dimensional structure that is rotationally symmetric with respect to the vertical centerline. The finite element mesh (Fig. 1) consists of six distinct regions representing the following components of a disc unit: (1) the vertebral body core of trabecular bone, (2) the vertebra's thin outer shell of cortical bone, (3) the bony end plate, (4) the nucleus pulposus, (5) the annulus fibrosis, and (6) the cartilagenous end plate. The nucleus pulposus was assumed to be incompressible, inviscid, and in a uniform state of pressure. Except where noted, the geometric sizing and material properties presented in the earlier study were also used here.

The inhomogeneity of the annulus is taken into account by varying the elastic coefficients, C_{ij}, according to the following relationship:

$$C_{ij}(r) = \frac{0.3C_{ij}(r_0)}{1-0.7(r/r_0)}, \tag{12}$$

where r and r_0 are the radial coordinate and outer radius of the disc, respectively. Sonnerup (1972) represented the variation of Young's modulus, $E(r)$, through the annulus by a similar relationship.

The load was applied by prescribing incremental uniform displacements at the top surface of the model. The bottom surface was restricted from vertical movement. The total load, F_a, divided by the disc–body interface area, A_i, is defined to be the applied pressure P_a. The actual pressure across the interface varies radially and is designated by P_a^*.

RESULTS AND DISCUSSION

The model was first utilized to determine representative values for the material constants and the constitutive parameter λ, so as to match the model behavior with reported experimental disc behavior. Next, it was used to study in detail the nonlinear behavior of normal discs under axial loading.

Determination of model parameters

The previously obtained anisotropic constants for the annulus fibrosis were utilized here. These material constants were obtained in the linear study so as to best match the following experimentally-determined behavior of an *L2/L3* disc: (1) ratio of applied pressure to nucleus pressure, and (2) ratio of disc bulge to disc compression. The anisotropy ratio was altered somewhat here so as to better match the nuclear pressure ratio over the entire load range. The numerical values of these constants at the periphery of the annulus obtained here along with previously reported values are presented in Table 1. The numerical values for the constants E_L, E_T, and G_{LT} for the nonlinear case cannot be interpreted without values of the strains because, as can be seen from equations (A.1–A.2), the nonlinear coefficient matrix is multiplied by a nonlinear function of the strains. Hence, to facilitate comparison, the ratios of the moduli are also included in the Table.

The nonlinear behavior of the annular material depends principally on the behavior of the collagenous fibers. It has been reported (Haut and Little) that the elastic component of stress for collagen is proportional to the square of the strain. This corresponds to a value of 1.5 for the constitutive parameter, λ. The effect of varying the parameter λ was studied by investigating the compressive response of an *L2/L3* disc. The gross behavior obtained for $\lambda = 1.5$ is in good agreement with that observed experimentally, so it was used in all further studies.

Table 1. Comparison between linear, nonlinear, and assumed degenerate material properties for the annulus fibrosis

Case	E_L (N/mm^2)	E_T (N/mm^2)	G_{LT} (N/mm^2)	E_L/E_T	G_{LT}/E_T	ν_{LT}
Linear at a load of 700 N	83.0	2.07	1.38	40.1	0.67	0.45
Nonlinear	1765.0	88.5	35.3	19.9	0.40	0.45
Degenerate nonlinear	180.0	88.5	35.3	2.0	0.40	0.45

Table 2. Ratio of nuclear pressure to applied pressure (at a load of 1000 N)

Disc Level	$T2/T3$	$T5/T6$	$T11/T12$	$L2/L3$	$L3/L4$	$L5/S1$
P_i/P_a	1.39	1.46	1.32	1.27	1.37	1.27

Behavior of model and comparison with reported experimental data

The compressive load–deflection curves of lumbar discs obtained from the model and the experimental curves of Brown *et al.*, Markolf, and Rolander are shown in Fig. 2. It can be seen that the material model chosen here is representative over a large range of loads. The predicted results agree well with those reported by Brown *et al.* and Markolf. Rolander's specimens were slightly stiffer. Perhaps the facets, which were not removed for his tests, contributed to the stiffnesses.

Model results for an $L2/L3$ disc indicate that the bulge is 1.9 times the axial deflection at a load of 1000 N. For an $L2/L3$ disc at a load of 1000 N, Brown *et al.* reported a value of 1.8 for the ratio of lateral bulge to axial compression and a value of 3.1 for the ratio of sagittal bulge to axial compression. Similarly, Rolander's data for an $L2/L3$ disc at a load of 1000 N indicates a value of 3.0 for the sagittal bulge ratio. Thus the model is also accurate in its prediction of deflections.

Results for thoracic discs obtained by using the same material properties are presented in Fig. 3 along with the experimental results of Markolf. The model results are in good agreement with these experiments. A comparison of the model load–deflection curves for different thoracolumbar discs shows that the discs become stiffer (i.e. the displacements become smaller for a given load level) as the level is increased from the $L3/L4$ disc to the $T5/T6$ disc and that the stiffness decreases from the $T5/T6$ level to the $T1/T2$ level. The mean experimental results reported by Markolf also show that the lumbar discs are softer than the lower thoracic ($T10/T11$ to $T12/L1$) and that the lower thoracic discs are softer than the mid-thoracic discs ($T7/T8$ to $T9/T10$). No experimental data for the upper thoracic discs are available for comparison.

The computed ratios of the internal nucleus pressure and the applied pressure, P_i/P_a, for different disc levels are reported in Table 2. The ratio at each level is relatively constant throughout the loading range. The lumbar values are in the range of 1.3–1.5, which is in agreement with the measurements of Nachemson (1960). Values for thoracic discs are not reported in the literature.

The normal stress distributions for an $L2/L3$ disc and a $T5/T6$ disc through the thickness of the annulus at the horizontal midplane are shown in Fig. 4. An examination of the differences in the stress distributions between the $L2/L3$ disc and the $T5/T6$ disc reveals a significant difference in their behavior. The normalized fiber stress, σ_{LL}, in the lumbar disc is tensile throughout and increases from its value at the inner boundary to a maximum value along the periphery; the normalized fiber stresses in the thoracic

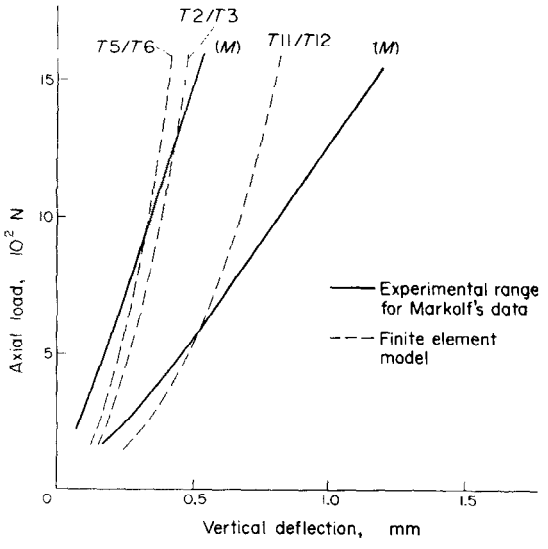

Fig. 3. Comparison between model-predicted and reported experimental thoracic load–deflection curves. Markolf's range is for discs $T7/T8$–$T9/T10$. Finite element results are for discs $T2/T3$, $T5/T6$, and $T11/T12$.

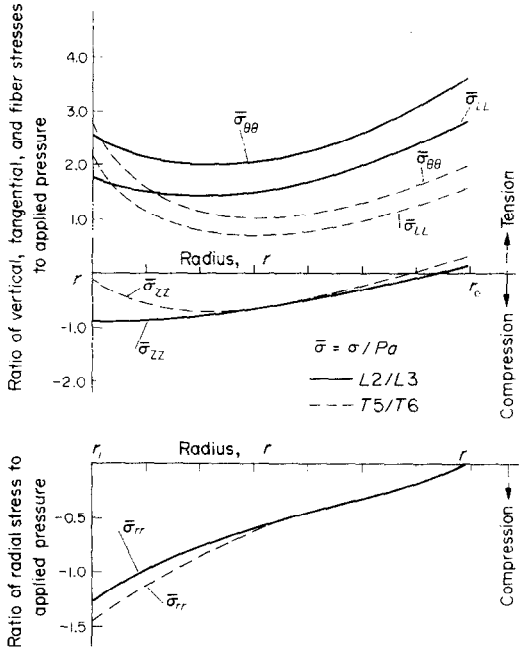

Fig. 4. Normalized stress distributions through the thickness of the annulus at the horizontal midplane for normal discs: $L2/L3$ and $T5/T6$.

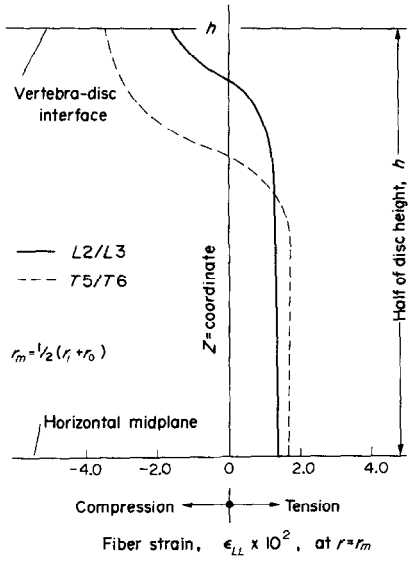

Fig. 5. Variation in fiber strain, as measured at annular mid-thickness (r_m), with z-coordinate. The difference in values between a $T5/T6$ disc and an $L2/L3$ disc is shown.

disc have lower values through the mid-annular region and are often compressive in larger regions above the mid-plane. The variation of fiber strain along the vertical coordinate, as shown in Fig. 5, shows that the collagen fibers are elongated throughout most of the $L2/L3$ disc. On the other hand, the fibers in a $T5/T6$ disc are compressed in a region near the vertebra.

This difference in behavior is related to the differences in the width to height ratios of thoracic and lumbar discs. Let us define an aspect ratio as the equivalent circular diameter divided by the height; these are given in Table 3. It can be seen that the aspect ratio of discs in the lumbar region are much smaller than in the upper thoracic region. Because of their greater relative height, lumbar discs behave essentially as medium-length, thick-walled tubes subjected to internal pressure with tensile hoop stresses dominant. In upper thoracic discs, on the other hand, the annulus is more constrained by the endplates: the hoop stress is less dominant and many of the annular fibers are in compression. Another difference between lumbar and thoracic discs is that the predicted thoracic load-deflected curves are more linear than the lumbar curves, even though the annular material in both is quite nonlinear. Markolf also reported that thoracic discs tend to behave more linearly than lumbar discs.

Because the predicted load–deflection curve for a thoracic disc is excessively stiff unless the difference between the tensile and compressive behavior of the annular material is taken into account, the parameter α defined in equations (A.2 and A.9) was used to reduce C_{11} in the presence of compressive strains. All results reported incorporate this modification.

The model was also used to study the disc under tensile loading. Since the nucleus is a fluid with negligible tensile or shear strength, it was assumed that the nucleus will not resist any tensile strains. Therefore, the nucleus was omitted from the model when tensile loading was studied. Figure 6 shows a comparison between the loading curves for compression and tension along with reported experimental results. The ratio of the final axial stiffness in compression to that in tension is 1.5; Markolf reported values from 1.5 to 3.0.

For the purpose of demonstrating the disc model behavior over the entire range of loads that has been tested experimentally, Fig. 7 shows the response of the $L3/L4$ disc model to axial loads from 3000 N tension to 6000 N compression. The computed results are compared to the experimental measurements of Brown *et al.* and one specimen measured by Markolf. The model predicts somewhat more nonlinearity than measured experimentally, but reproduces the difference between compressive and tensile behavior quite well. Under both compressive and tensile loads, the fiber strain in the midplane of the disc is extensional: at 6000 N compression, the fiber strain is about 4%, while at 3000 N tension the fiber strain is also approx. 4%. It is of interest that these strains are well within the extensibility range of collagenous fibers, which is consistent with the experimental finding that discs sustain little or no damage when a motion segment is tested to failure in compression.

Disc degeneration studies

During a lifetime, a disc undergoes morphological changes which influence the mechanical properties and mechanical function of the disc's components. Some of these changes were incorporated in the model and their effect on the gross behavior studied. For instance, the nucleus pulposus undergoes a loss

Table 3. Aspect ratio for intervertebral discs

Disc level	Equivalent circular dia., D(cm)	Disc height, H(cm)	D/H
$T2/T3$	2.58	0.31	8.3
$T5/T6$	2.82	0.26	10.8
$T11/T12$	3.84	0.68	5.6
$L2/L3$	4.26	1.14	3.7
$L3/L4$	4.42	1.22	3.6
$L5/S1$	4.40	1.57	2.8

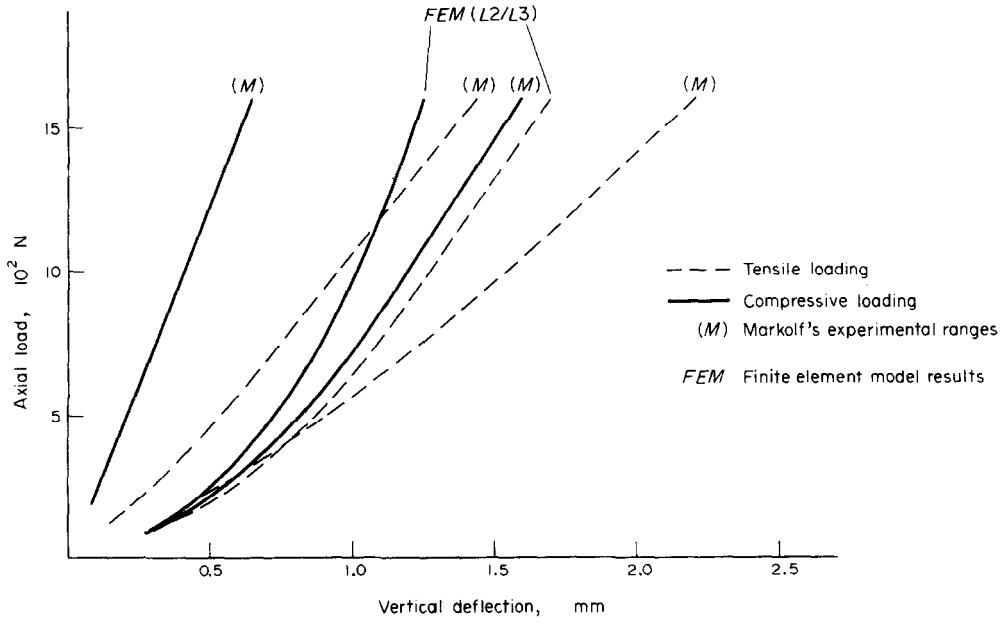

Fig. 6. Difference between tensile and compressive behavior of lumbar discs are shown. A comparison between experimental results for disc levels $L1/L2$ and $L2/L3$, as reported by Markolf, and model-predicted results for an $L2/L3$ disc is illustrated.

of water content with age. According to Püschel (1930), water content is 88% by wt at birth and 69% at age 77. Beadle reports that in extreme cases of degeneration, the nucleus loses its fluid characteristic and becomes desiccated. An example of this type of degeneration was simulated in the model by considering the nucleus to be void while the material properties of the annulus fibrosis were assumed to be unaltered. Figures 2 and 8 show the reduction in disc stiffness and the resulting stress distribution through the annulus, respectively. The reduced stiffness is easily explained by examining the stress distributions. The absence of a nucleus–annulus interaction changes

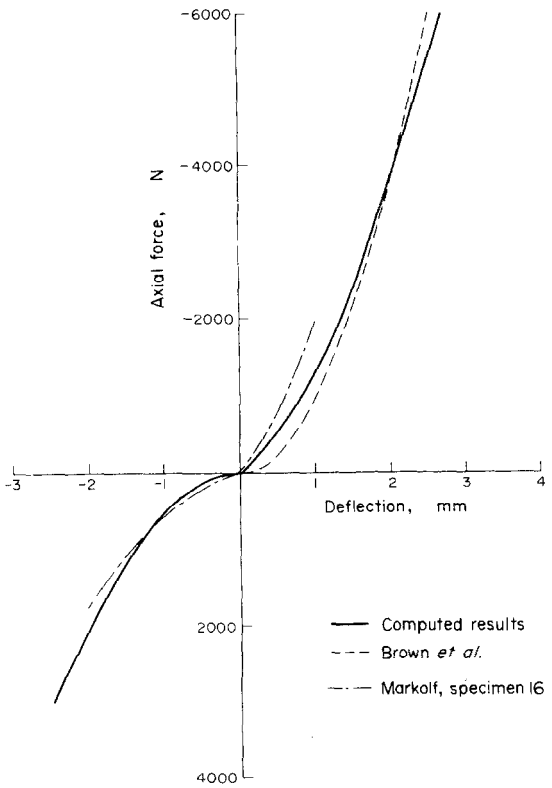

Fig. 7. Comparison of computed tensile and compressive behavior with experimental results. Computed results and Brown results are interchanged for axial force less than zero.

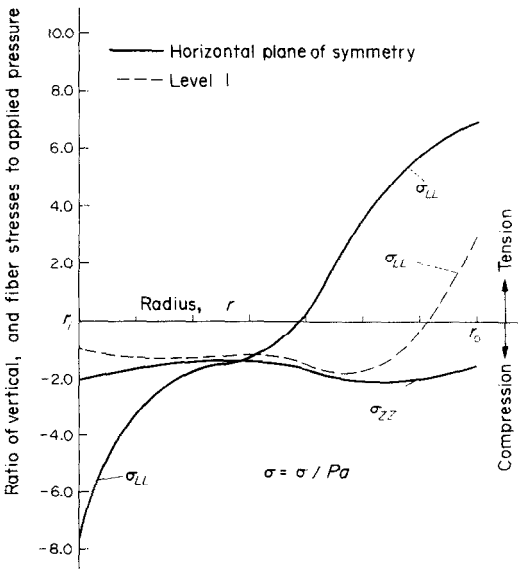

Fig. 8. Normalized stress distributions through the thickness of the annulus for a denucleated $L2/L3$ disc (the two levels are indicated in Fig. 1). σ_{LL} is the normal stress acting along the fiber direction, and σ_{zz} is the normal stress acting in the z-direction.

the behavior of the disc from an internally pressurized thick-walled tube with considerable tensile hoop stress to a thick ring under axial compression with very little tensile hoop stress. The collagen fibers, which have strong resistance only in tension, act compressively when the annulus is absent and hence are relatively ineffective in resisting the load.

Another form of degeneration is characterized by radial tears in the annulus fibrosis (Farfan *et al.*, 1972). This type of degeneration was modeled in these studies by reducing the effective elastic modulus in the fiber direction; this scheme was also employed in the previous study. The resulting elastic coefficient values are shown in Table 1. Since the reduced values were chosen arbitrarily, the results only have qualitative significance. The reduced value chosen would correspond to a considerable reduction in the elastic modulus; thus, it represents a severely torn annulus. The model predicts that the change in the load–deflection curve (Fig. 2) produced by annular tears is not as drastic as that produced by denucleation. Since only minor changes in the normalized stress distributions occurred between the present study of annular degeneration and the previous one, these results are not presented here.

SUMMARY AND CONCLUSIONS

A nonlinear stress–strain relation for representing the time independent behavior of annular material has been proposed. Incorporation of the relation into an existing finite element model yields results which are in good agreement with available experimental studies, such as bulging, nuclear pressure, and level to level variations.

These studies have yielded several interesting findings on the behavior of the intervertebral discs: (1) although the elastic response of the annulus fibrosis is quite nonlinear, the increase in volume of the compressed zones with increasing load causes the overall response of thoracic discs to be nearly linear; (2) the stress distributions in thoracic and lumbar discs differ substantially, with hoop stresses more dominant in the lumbar discs; and (3) the computed stiffness of a lumbar disc decreases by a factor of about 2 if the nucleus is absent, indicating that the nucleus plays a significant role in carrying compressive axial loads.

These studies have also shown the importance of including the nonlinear material behavior in the analysis of the mechanical function of soft tissue structures, such as the disc. Although a basic understanding can often be gained with less complex, linear models, the predictive value of linear models is severely limited because they are restricted to small load ranges. This was illustrated by the marked difference in the response to tension and compression and in the absence of the nucleus. Thus the analysis of the intervertebral disc over the normal *in vivo* range of loading requires the inclusion of the nonlinear material behavior.

A knowledge of the stresses associated with various lifting motions and other mechanical functions is of considerable importance in understanding the relationships between occupational activities and chronic back injuries. Since the determination of strains and stresses in cadaver discs is almost out of the question experimentally, models of this type are essential if mechanical functions are to be related to injury mechanisms in the disc. Because of the tremendous variability of tissue properties among individuals, the predictive capability of such biomechanical models is more limited than e.g., models of metallic structures. However, if a model is reasonably representative of typical tissue behavior, it can nevertheless provide significant insight into injury mechanisms.

The present computational model can only treat tension–compression and cannot treat flexion–extension, lateral bending or torsion. However the material properties obtained here are applicable to more complex models which can treat these motions. Thus, these nonlinear stress–strain relations should prove useful in further studies of disc behavior.

Acknowledgement—This research was supported in part by Public Health Service Grant OH 00514 from the National Institute for Occupational Safety and Health, by Public Health Service Grant AM 15575 and Development Award AM 00029 from the National Institute of Arthritis, Metabolism, and Digestive Diseases.

REFERENCES

Beadle, O. A. (1931) The intervertebral disc. Observations on their normal and morbid anatomy in relation to certain spinal deformities. Medical Research Council. Special report series. HMSO, London, No. 161.

Belytschko, T. B., Andriacchi, T. P., Schultz, A. B. and Galante, J. O. (1973) Analog studies of forces in the human spine: computational techniques. *J. Biomechanics* **6**, 361–371.

Belytschko, T. B. and Kulak, R. F. (1973) A finite element method for a solid enclosing an inviscid, incompressible fluid. *J. Appl. Mech.* **40** (2); *Trans. ASME* **95** E, 609–610.

Belytschko, T. B., Kulak, R. F., Schultz, A. B. and Galante, J. O. (1974) Finite element stress analysis of an intervertebral disc. *J. Biomechanics* **7**, 277–285.

Blatz, P. J. (1969) On the mechanical behavior of elastic animal tissue. *Trans. Soc. Rheol.* **13**, 83–102.

Brown, T., Hansen, R. J. and Yorra, A. J. (1957) Some mechanical tests on the lumbosacral spine with particular reference to the intervertebral disc. *J. Bone Jnt Surg.* **39A**, 1135–1164.

Elden, H. R. (1968) Physical properties of collagen fibers. *Int. Rev. Conn. Tissue* **4**.

Farfan, H. F., Huberdeau, R. M. and Dubow, H. I. (1972) Lumbar intervertebral disc degeneration. *J. Bone Jnt. Surg.* **54A**, 492–510.

Fick, R. (1904–1911) *Handbuch der Anatomie und Mechanik der Gelenke unter Berücksichtigung der bewegenden Muskeln*. Fischer, Jena.

Fung, Y. C. B. (1965) Generalized Hooke's Law. *Foundations of Solid Mechanics*, pp. 127–128. Prentice-Hall, N.J.

Fung, Y. C. B. (1968), Biomechanics (its scope, history, and some problems of continuum mechanics in physiology). *Appl. Mech. Rev.* **21**(1), 1–20.

Galante, J. O. (1967) Tensile properties of the human lumbar annulus fibrosis. *Acta Orthop. Scand.* Suppl 100.

Haut, R. C. and Little, R. W. (1972) A constitutive equation for collagen fibers. *J. Biomechanics* **5**, 423–430.
Horton, W. G. (1958) Further observations in the elastic mechanism of the intervertebral disc. *J. Bone Jnt Surg.* **40B**, 552–557.
Jayne, B. A. and Suddarth, S. K. (1966) Matrix-tensor mathematics in orthotropic elasticity. Orientation effects in the mechanical behavior of anisotropic structural materials. ASTM STP 405, Am. Soc. Testing Matls., 39–58.
Kraus, H., Farfan, H. F. and Jones, Jr., T. J. (1972) Stress analysis of human intervertebral discs. *25th ACEMB*, 242.
Markolf, K. L. (1972) Deformation of the thoracolumbar intervertebral joints in response to external loads. *J. Bone Jnt Surg.* **54A**, 511–533.
Mitton, R. G. (1945) Mechanical properties of leather fibers. *J. Int. Soc. Leath. Tr. Chem.* **29**, 169–194.
Morgan, F. R. (1960) The mechanical properties of collagen fibers: stress–strain curves. *J. Soc. Leath. Tr. Chem.* **44**, 170–182.
Nachemson, A. (1960) Lumbar intra-discal pressure. *Acta Orthop. Scand.*, Suppl. 43.
Noble, B. (1960) Definite quadratic forms. In *Applied Linear Algebra*, pp. 392–396, Prentice-Hall, N.J.
Oden, J. T. (1972) *Finite Elements of Nonlinear Continua*. McGraw-Hill, New York.
Püschel, J. (1930) Der Wassergehalt normaler und degenerierter Zwischenwirbelscheiben. *Beitr. Path. Anat.* **84**, 123–130.
Rolander, S. D. (1969) Motion of the lumbar spine with special reference to the stabilizing effect of posterior fusion. *Acta Orthop. Scand.*, Suppl. 90.
Sonnerup, L. (1972) A semi-experimental stress analysis of the human intervertebral disc in compression. *Exp. Mech.* **12**, 142–147.
Virgin, W. J. (1951) Experimental investigations into the physical properties of the intervertebral disc. *J. Bone Jnt. Surg.* **33B**, 607–611.
Wissman, J. W. (1965) Nonlinear structural analysis-tensor formulation. Proc. Conf. on Matrix Methods in Structural Mech., AFFDL-TR-66-80, 679–696.
Zienkiewicz, O. C. (1971) Element characteristics. In *The Finite Element Method in Engineering Science*, pp. 74–83, McGraw-Hill, New York.

APPENDIX A

This Appendix gives a detailed development of the elastic constants in equation (8). Both the orthotropy of the annulus and the dependence of stiffness on fiber strain are taken into account. In order to include these features, the stress–strain law is first expressed in a Cartesian coordinate system $(\tilde{x}_1, \tilde{x}_2, \tilde{x}_3)$, in which at any point, $\tilde{x}_1$ is along the fiber direction, $\tilde{x}_2$ in the plane of the lamella, and $\tilde{x}_3$ perpendicular to the plane. The lamella is then orthotropic, with $\tilde{x}_1$ an axis of transverse isotropy. The three dimensional stress–strain law may be written as

$$\tilde{\sigma}_i = 2\lambda K^{\lambda-1}\tilde{C}_{ij}\tilde{\epsilon}_j, \tag{A.1}$$

where $\tilde{C}_{ij}$ has the same form as the orthotropic, linear relations given by Jayne and Suddarth (1966). Writing out all the terms in the matrices in the above equations, we have

$$\begin{Bmatrix} \tilde{\sigma}_{11} \\ \tilde{\sigma}_{22} \\ \tilde{\sigma}_{33} \\ \tilde{\sigma}_{12} \\ \tilde{\sigma}_{13} \\ \tilde{\sigma}_{23} \end{Bmatrix} = \frac{2\lambda K^{\lambda-1}}{D} \begin{bmatrix} \alpha E_1(1 - \nu_{32}\nu_{23}) & E_1(\nu_{12} + \nu_{32}\nu_{13}) & E_1(\nu_{13} + \nu_{12}\nu_{23}) & 0 & 0 & 0 \\ & E_2(1 - \nu_{13}\nu_{31}) & E_2(\nu_{23} + \nu_{13}\nu_{21}) & 0 & 0 & 0 \\ & & E_3(1 - \nu_{12}\nu_{21}) & 0 & 0 & 0 \\ & & & \tfrac{1}{2}DG_{12} & 0 & 0 \\ & & & & \tfrac{1}{2}DG_{13} & 0 \\ \text{symmetric} & & & & & \tfrac{1}{2}DG_{23} \end{bmatrix} \begin{Bmatrix} \tilde{\epsilon}_{11} \\ \tilde{\epsilon}_{22} \\ \tilde{\epsilon}_{33} \\ 2\tilde{\epsilon}_{12} \\ 2\tilde{\epsilon}_{13} \\ 2\tilde{\epsilon}_{23} \end{Bmatrix} \tag{A.2}$$

where

$$D = 1 - 2\nu_{12}\nu_{23}\nu_{31} - \nu_{13}\nu_{31} - \nu_{12}\nu_{21} - \nu_{23}\nu_{32} \tag{A.3}$$

and as a result of transverse isotropy

$$\begin{aligned} E_1 &= E_L \\ E_2 &= E_3 = E_T \\ \nu_{21} &= \nu_{31} = \nu_{LT} \\ G_{13} &= G_{12} = G_{LT} \\ G_{23} &= \frac{E_T}{2(1 + \nu_{23})}, \end{aligned} \tag{A.4}$$

where E_L and E_T are the longitudinal and transverse moduli, G_{LT} the shear modulus, and ν_{LT} a Poisson's ratio. The remaining Poisson's ratios are obtained by the reciprocal relations

$$\nu_{ij}E_i = \nu_{ji}E_i \quad \text{(no sum)} \tag{A.5}$$

and the conditions

$$1 - (\nu_{13} + \nu_{23}) = \delta_1 \geq 0 \tag{A.6a}$$

$$1 - (\nu_{12} + \nu_{32}) = \delta_2 \geq 0 \tag{A.6b}$$

$$1 - (\nu_{21} + \nu_{31}) = \delta_3 \geq 0. \tag{A.6c}$$

where $\delta_i = 0$ for incompressible materials. For transversely isotropic materials, equations (A.6) may be written in the form

$$1 - \frac{E_T}{E_L}\nu_{LT} - \nu_{23} = \delta_1 \tag{A.7a}$$

$$1 - \frac{E_T}{E_L}\nu_{LT} - \nu_{23} = \delta_2 \tag{A.7b}$$

$$1 - 2\nu_{LT} = \delta_3. \tag{A.7c}$$

It can be seen that equations (A.7a and b) are identical, so that we are left with two compressibility conditions. If we add the requirements that Poisson's ratios must be positive, we have the conditions

$$\begin{aligned} 0 \leq \nu_{LT} &= 0.5 - \tfrac{1}{2}\delta_3 \\ 0 \leq \nu_{23} &= 1 - \frac{E_T}{E_L}\nu_{LT} - \delta_2 \end{aligned} \tag{A.8}$$

with δ_2 and δ_3 vanishing for an incompressible material. Since incompressible materials cannot be treated in the standard stiffness method of analysis, the δ_i were taken to be 0.1.

The factor α in equation (A.2) is given by

$$\alpha = \begin{cases} 0.3 \text{ when } \tilde{\epsilon}_{11} < 0 \text{ (fibers in compression)} \\ 1.0 \text{ when } \tilde{\epsilon}_{11} \geq 0 \text{ (fibers in tension)} \end{cases} \tag{A.9}$$

and is introduced to reflect the reduced stiffness of the lamella when its fibers are compressed; the particular value used here was obtained by matching overall disc response. It would appear to be more suitable to introduce this difference into the longitudinal modulus E_L; however this is not acceptable because E_L appears in off diagonal terms in $\tilde{C}_{ij}$, so the tension stiffness reduction would yield discontinuous elastic coefficients $\tilde{C}_{ij}$, $i \neq j$, and hence a nonunique stress–strain law. As an illustration of this statement, consider a state of strain with $\tilde{\epsilon}_{22} > 0$ and $\tilde{\epsilon}_{11}$ passing

from positive to negative. If $\tilde{C}_{12}$ is a discontinuous function of $\tilde{\epsilon}_{11}$, then $\tilde{\sigma}_{22}$ and $\tilde{\sigma}_{11}$ would be discontinuous as $\tilde{\epsilon}_{11}$ passes through zero. Hence if the stiffness is reduced when a single strain becomes tensile, only the diagonal terms of $\tilde{C}_{ij}$ matrix may be discontinuous functions of the strain.

Because of the axisymmetry of the problems considered here, the fibers in alternating lamellae in the neighborhood of a given point will both be either in tension or compression. On the other hand, for three dimensional loading conditions, it is possible for the fibers in one lamella to be in tension while those of the adjacent lamella are in compression. It should also be noted that because of the factor α in equation (A.2), the constants E_L, E_T, ν_{LT} and G_{LT} pertain to the respective moduli only when the fibers are in tension.

The elastic constants in the cylindrical coordinates as given in equation (8) are obtained by transforming the elastic coefficients into the cylindrical coordinates and averaging the coefficients of adjacent lamellae. For clarity, these relations are written in matrix notation as follows

$$[C] = \tfrac{1}{2}([R(\phi)]^T[\tilde{C}][R(\phi)] + [R(-\phi)]^T[\tilde{C}][R(-\phi)]), \tag{A.10}$$

where

$$[R(\phi)] = \begin{bmatrix} 0 & c^2 & s^2 & 0 \\ 0 & s^2 & c^2 & 0 \\ 1 & 0 & 0 & 0 \\ 0 & -cs & cs & 0 \\ 0 & 0 & 0 & s \\ 0 & 0 & 0 & c \end{bmatrix} \tag{A.11}$$

$$s = \sin\phi \qquad c = \cos\phi$$

and ϕ is the angle between the fiber and circumferential directions. This transformation is based on the assumption that the plane of each lamella is perpendicular to the $r - \theta$ plane, and thus neglects their small inclination. The matrix [C] computed from equation (A.10) is used in the axisymmetric finite element program.

APPENDIX B

Computational technique

Since the nonlinear behavior of the annulus fibrosis was incorporated explicitly in this study, the computational procedure used by Belytschko *et al.* (1974) was modified to account for material nonlinearity.

The development of finite element equations for this system of compressible elements enclosing an incompressible, hydrostatic fluid is developed in Belytschko and Kulak (1973). The governing equation is

$$\{F^{ext}\} = \{F^{int}\}, \tag{B.1}$$

where $\{F^{ext}\}$ are the nodal loads due to the applied loads and

$$\{F^{int}\} = \sum_e [L^{(e)}]^T \int_{V^{(e)}} [B]^T\{\sigma\}\, dV + p\{T\}, \tag{B.2}$$

where the summation is taken over all compressible elements, $V^{(e)}$ is the volume of element e, $[L^{(e)}]$ is the connectivity matrix (see Oden, 1972), $\{T\}$ is the matrix which relates the volume change of the incompressible region to the nodal displacements (see Belytschko and Kulak), and $[B]$ is the strain, nodal displacement matrix defined by

$$\{\epsilon\} = [B]\{D^{(e)}\} = [B][L^{(e)}]\{D\}, \tag{B.3}$$

where $\{D^{(e)}\}$ and $\{D\}$ are the element and total nodal displacement matrices. The stresses are related to the strains by equation (A.6). Except for the second term in equation (B.2), which is associated with the incompressible region, this system of equations is equivalent to the standard finite element equations; details of these equations may be found in Zienkiewicz (1971).

Because of the nonlinearity of the stress–strain relations, the governing equations (B.1), when expressed in terms of the nodal displacements, are nonlinear. For purposes of solving these equations, an incremental linearization technique with equilibrium checks was used. This has been described by Wissman (1965) and used by Belytschko *et al.* (1973) in the nonlinear static analysis of the human spine.

In this procedure, the load is subdivided into increments $\{\Delta F^{ext}\}$ and the equations of equilibrium are linearized; the linearized equations of equilibrium in this case are

$$[K]\{\Delta D\} + \{T\}\,\Delta p = \{\Delta F^{ext}\}. \tag{B.4a}$$

In addition, the condition that the nucleus is incompressible,

$$\{T\}^T\{\Delta D\} = 0 \tag{B.4b}$$

must be satisfied. Here $[K]$ is the tangential stiffness given by

$$[K] = \sum_e [L^{(e)}]^T \int_{V^{(e)}} [B]^T[C^t][B]\, dV[L^{(e)}] \tag{B.5}$$

and $[C^t]$ is given by equations (A.10 and A.11). By combining equations (B.4a and B.4b), it can be shown that

$$\Delta p = \frac{\{T\}^T[K^{-1}]\{\Delta F^{ext}\}}{\{T\}^T[K^{-1}]\{T\}}. \tag{B.6}$$

By simultaneously solving the stiffness equations with right hand sides $\{\Delta F^{ext}\}$ and $\{T\}$, we obtain $\{X_1\}$ and $\{X_2\}$ defined by

$$\{X_1\} = [K^{-1}]\{\Delta F^{ext}\} \tag{B.7}$$

$$\{X_2\} = [K^{-1}]\{T\}. \tag{B.8}$$

Then

$$\Delta p = \frac{\{T\}^T\{X_1\}}{\{T\}^T\{X_2\}} \tag{B.9}$$

while from equation (B.3) it follows that

$$\{\Delta D\} = \{X_1\} - \Delta p\{X_2\}. \tag{B.10}$$

The equilibrium check is accomplished as follows. The displacement increment $\{\Delta D\}$ is added to the sum of all previous increments to obtain the total displacements, and the pressure increment is added to the sum of the previous increments. The displacements are used to compute the strains and stresses by equations (B.3 and A.6) respectively. The internal forces are then computed by equation (B.2), in terms of these stresses and the total pressure. The discrepancy in equilibrium is checked by computing an error force matrix

$$\{F^{err}\} = \{F^{ext}\} - \{F^{int}\}. \tag{B.11}$$

If this error force does not meet a specified tolerance, equation (B.7) is resolved with only the error loads applied; otherwise, the next increment of load is added and the procedure is repeated.